

---

# A ROBUST BACKPROPAGATION-FREE FRAMEWORK FOR IMAGES

---

**Timothy Zee**

Rochester Institute of Technology  
Rochester, NY 14623, USA  
tsz2759@rit.edu

**Alexander G. Ororbia\***

Rochester Institute of Technology  
Rochester, NY 14623, USA  
ago@cs.rit.edu

**Ankur Mali**

The Pennsylvania State University  
State College, PA 16801, USA  
aam35@psu.edu

**Ifeoma Nwogu\***

University at Buffalo, SUNY  
Buffalo, NY 14260, USA  
inwogu@buffalo.edu

## ABSTRACT

While current deep learning algorithms have been successful for a wide variety of artificial intelligence (AI) tasks, including those involving structured image data, they present deep neurophysiological conceptual issues due to their reliance on the gradients computed by backpropagation of errors (backprop) to obtain synaptic weight adjustments; hence are biologically implausible. We present a more biologically plausible approach, the error-kernel driven activation alignment (EKDA) algorithm, to train convolution neural networks (CNNs) using locally derived error transmission kernels and error maps. We demonstrate the efficacy of EKDA by performing the task of visual-recognition on the Fashion MNIST, CIFAR-10 and SVHN benchmarks as well as conducting blackbox robustness tests on adversarial examples derived from these datasets. Furthermore, we also present results for a CNN trained using a non-differentiable activation function. All recognition results nearly matches that of backprop and exhibit greater adversarial robustness compared to backprop.

## 1 Introduction

In order for the brain to learn from sensory patterns, the synaptic connections between the neurons need to be modified [1, 2]. Although neurophysiologists have made great progress in characterizing the mechanisms involved in single synapse transmissions, according to Südhof and Malenka [3], in their classical paper about the past, present and future of neuron studies, the most daunting challenge to neuroscientists is still the understanding of how the neurons in the complex, synaptic network of the brain work together and adjust their synapses to accomplish goals. While artificial neural networks (ANNs) trained by backpropagation of errors (backprop) present a practical, feasible implementation of learning by synaptic adjustment, it is largely regarded by neuroscientists as biologically implausible for various reasons, including the implausibility of the direct backwards propagation of error derivatives for synaptic updates - this is considered a deep conceptual issue [4]. Rather, it is more likely that neural activity differences, driven by feedback connections, are used in locally effecting synaptic changes [5]. This overcomes backprop's major implausibilities in a way that is both natural and compatible with the current understanding of how brain circuitry operates.

Although a few classes of algorithms have been proposed to address the specific challenge of error gradient propagation in training ANNs, fewer still have been proposed to handle the highly structured data found in large-scale images datasets. Current-day convolutional neural networks (CNNs) continue to set the benchmark standards for difficult vision problems [6, 7] and they do so using a backprop-driven approach that requires having symmetric weight matrices in both the feedforward and feedback pathways. More importantly, they

---

\*Equal advising.

also require a global feedback pathway to carry back update signals from the output back towards the input, one of the key causes of the vanishing/exploding gradient problems [8, 9].

In this work, we introduce a more biologically-plausible error synaptic feedback mechanism that we call the (learnable) *error-kernel*, which will generate target activities for the feature maps within a CNN to align to. We call this learning mechanism *error-kernel driven activation alignment (EKDA*A). In our learning scheme, the forward pathway relies on traditional weight matrices whereas the backward pathway focuses on error kernels and maps, thus eliminating the symmetric weight structure inherent to backprop-trained networks (resolving the weight transport problem). We analyze the resulting neural system’s learning capacity as well as its robustness on real image datasets and present our empirical findings.

EKDA

A notably opens the door to a wider variety of neural structures, such as those that use lateral neural connections, where forward/backward propagation no longer carries the traditional meaning. Additionally, our framework marks a step forward towards designing networks that are less-constrained to appease backprop (which imposes restrictions such as the need for differentiable activities) and instead focus more completely on designing for the task/problem at hand. We demonstrate this by successfully training a convolutional network on image data, using the signum function (which has a derivative of zero everywhere except at zero, i.e., a Dirac delta function).

**Credit assignment and artificial neural network learning:** The credit assignment problem has to do with determining how the success of the overall system can be attributed to the contributions of its various components [10]. Although Hebbian learning [2] is one of the earliest and simplest biologically plausible learning rules for addressing the credit assignment problem in ANNs, extending them to the CNN has not yet been well-developed. Our proposed approach aims to fill this gap.

## 2 Related Work

In this section, we discuss several classes of approaches built on the premise of biologically-plausible learning rules that do not involve back-propagating computed derivatives/gradients through all layers of the ANN.

**The Bottleneck Approach:** One of the more recent efforts in this area, inspired by information theory, is the Hilbert-Schmidt independence criterion (HSIC) bottleneck training algorithm [11], based on the Information Bottleneck (IB) principle [12]. HSIC performs credit assignment locally and layer-wise, seeking hidden representations that have high mutuality with targets but less with the inputs to that layer (based on information propagated from the layer below). Approaches based on the bottleneck mechanism are considered to be the least bio-plausible. Others [13] have proposed variants that use an evolution strategy to search for optimal weights without gradient descent. However, these approaches often struggle with slow convergence and require many iterations to find optimal solutions.

**Feedback Alignment:** Previously, an algorithm named *Random Feedback Alignment (RFA)* was proposed in [14], where it was argued that the use of the transpose of the forward weights ( $\mathbf{W}^\ell$  for any layer  $\ell$ ) in backprop, meant to carry backwards derivative information, was not required for learning. Rather, they showed that network weights could be trained by replacing the transposed forward weights with fixed, random matrices of the same shape ( $\mathbf{B}^\ell$  for layer  $\ell$ ), ultimately side-stepping the weight transport problem [15].

Direct Feedback Alignment (DFA) [16], and its variants [17, 18, 19], was inspired by RFA [14], but in contrast to RFA, it directly propagates the error signal to individual layers, rather than layer-wise as done in RFA. Across multiple neural architectures, it was observed that networks trained with DFA showed a steeper reduction in the classification error when compared to those trained with backprop.

To compare these biologically-plausible feedback alignment-based training paradigms with EKDA

A, we extended the corresponding published works and implemented CNN versions of FA, DFA, and other related variants. Details of their performance on benchmark image datasets are given in Section 4 .

**Target Propagation:** Target propagation (target prop or TP) [20] is another approach to credit assignment in deep neural networks, where the goal is to compute targets that are propagated backwards to each layer of the network. Target prop essentially designs each layer of the network as an auto-encoder, with the decoder portion attempting to learn the inverse of the encoder (modified by a linear correction to account for the imperfection of the auto-encoders themselves). This corrected difference (between encoder and decoder) is propagated throughout the network. This process allows difference target prop (DTP) [20] and variants [21, 9] (e.g., DTP- $\sigma$ ) to side-step the vanishing/exploding gradient problem. However, TP approaches are expensive

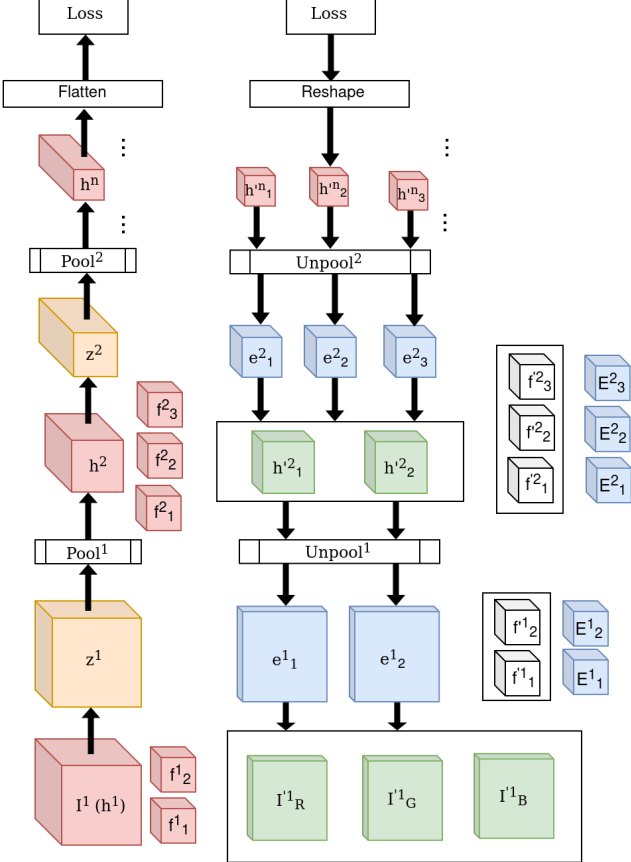


Figure 1: EKDA forward and backward updates. Forward propagation convolves the current pathway with applicable filters (in red) and then continues on to the next layer (in orange). To propagate error from layer  $\ell$  to  $\ell - 1$ , backprop computes a circular convolution of  $\mathbf{z}^n$  on  $\mathbf{f}^n$  to translate the signal to  $\ell - 1$ . EKDA uses error map  $\mathbf{e}^n$  and computes a circular convolution on  $\mathbf{E}^n$  to create the signal pathway for  $\ell$ . In a layer-wise update, tensors used to continue the signal pathway backwards are shown in blue and their resulting layers are shown in green.

and can be unstable, requiring multiple forward/backward passes in each layer-wise encoder/decoder in order to produce targets.

**Representation Alignment:** *Local Representation Alignment (LRA)* [22] and recursive LRA [23] represent yet another class of credit assignment methods, inspired by predictive coding theory [24] and similar in spirit to target prop. Under LRA, each layer in the neural network has a target associated with it such that changing the weights in a particular layer will help move layer-wise activity towards better matching a target activity value. LRA was shown to perform comparably to backprop for fully-connected models, but extending/applying it to vectorized natural images like CIFAR-10 resulted in significant performance degradation.

In contrast to TP and LRA approaches, our proposed algorithm, EKDA, the forward and backward activities share as minimal information as possible; this helps the model to better overcome poor initialization and stabilization issues that might arise during training. Furthermore, EKDA naturally works well with systems based on convolution.

### 3 Error Kernel Credit Assignment

In implementing EKDA, the forward pass in the CNN remains the same, however, the backward pass uses a form of Hebbian learning that locally computes error kernels and aims to align the forward activations accordingly.

**Notation:** We denote standard convolution with the symbol  $*$  and deconvolution with symbol  $\circlearrowleft$ . Hadamard product is denoted by  $\odot$  while  $\cdot$  represents a matrix/vector multiplication.  $(\cdot)^T$  denotes the transpose operation.

$\text{Flip}(\mathbf{X})$  is a function for flipping a tensor and is defined as taking the transpose of  $\mathbf{X}$  over both the x-axis and y-axis such that the value of an element  $\mathbf{X}_{i,j}$  after flipping results in the location  $\mathbf{X}_{n-i,n-j}$ .  $\text{Flatten}(\mathbf{z})$  means that the input tensor  $\mathbf{z}$  is converted to a column vector with rows equal to the number of elements it contained while  $\text{UnFlatten}(\mathbf{z})$  is its inverse (converts the vector back to its original tensor shape).

We use the notation  $:$  to indicate extracting a slice of a certain dimension in a tensor object, i.e.,  $\mathbf{V}_{j,:,:}$  means that we extract all scalar elements in the  $j$ th slice of the three dimensional tensor  $\mathbf{V}$ . Finally,  $=$  denotes equality while  $\leftarrow$  denotes variable assignment.

**Inference Dynamics:** Given an input (color) image  $\mathbf{x}$ , inference in a basic CNN consists of running a feedforward pass through the underlying model, computing the activities (or nonlinear feature maps) for each layer/level  $\ell$ , where the the model contains  $L_C$  convolutional layers total. The CNN is parameterized by a set of synaptic tensors  $\Theta = \{\mathbf{W}^1, \mathbf{W}^2, \dots, \mathbf{W}^L, \mathbf{W}_y\}$  where the last parameter  $\mathbf{W}_y$  is a two-dimensional tensor (or matrix) meant to be used in a softmax/maximum entropy classifier. All other tensors  $\mathbf{W}^\ell, \ell = 1, 2, \dots, L$  are four-dimensional and of shape  $\mathbf{W}^\ell \in \mathcal{R}^{N_{\ell-1} \times N_\ell \times h_\ell \times w_\ell}$ . This means that any tensor  $\mathbf{W}^\ell$  houses  $N_\ell$  sets of  $N_{\ell-1}$  filters/kernels of shape  $h_\ell \times w_\ell$ . Note that the bottom tensor  $\mathbf{W}^0$ , which takes in as input the source image, would be of shape  $\mathbf{W}^0 \in \mathcal{R}^{N_0 \times N_1 \times h_0 \times w_0}$  where  $N_0$  is the number of input color channels, e.g., three, for images of size  $h_0 \times w_0$  pixels.

The  $m$ th feature map of any convolutional layer  $\ell$  is specifically calculated as a function of the  $N_{\ell-1}$  features maps of the layer below ( $n \in N_{\ell-1}$  – there are  $N_{\ell-1}$  input channels to the  $m$ th channel of layer  $\ell$ ). This is done, with  $\mathbf{h}_{:, :, m}^\ell$  initialized as  $\mathbf{h}_{:, :, m}^\ell = \mathbf{0}$ , in the following manner (bias term omitted for clarity):

$$\mathbf{h}_{m, :, :}^\ell \leftarrow \mathbf{h}_{m, :, :}^\ell + \mathbf{W}_{m, n, :, :}^\ell * \mathbf{z}_{n, :, :}^{\ell-1}, \forall n \quad (1)$$

$$\mathbf{z}_{m, :, :}^\ell = \phi^\ell(\mathbf{h}_{m, :, :}^\ell) \quad (2)$$

where  $\mathbf{W}_{m, n, :, :}^\ell$  denotes the specific filter/kernel that is applied to input channel  $n$  when computing values for the  $m$ th output channel/map. Note that  $\phi^\ell$  is the activation function applied to any output channel in layer  $\ell$ , e.g.,  $\phi^\ell(v) = \max(0, v)$ . Max (or average) pooling is typically applied directly after the nonlinear feature map/channel has been computed, i.e.,  $\mathbf{z}_{m, :, :}^\ell \leftarrow \Phi_{mp}(\mathbf{z}_{m, :, :}^\ell)$ .

**Learning Dynamics:** Once inference has been conducted, we may then compute the values needed to adjust the filters themselves. To calculate the updates for each filter in the CNN, EKDA proceeds in two steps: 1) calculate target activity values for each feature map in each layer – this is then used to compute the error neurons (or error neuron maps), a type of neuron specialized for computing mismatch signals inspired by predictive processing brain theory [24], and, 2) calculate the updates/adjustments for each filter given the error neuron values. To do so, we introduce a specific set of filter parameters that we call the *error kernels*, each denoted as  $\mathbf{E}_{m, n, :, :}^\ell$ , for every map and layer in the CNN. This means that, if we include these error kernels as part of the parameter set of the CNN learned by EKDA,  $\Theta = \{\mathbf{W}^0, \mathbf{E}^0, \mathbf{W}^1, \mathbf{E}^1, \dots, \mathbf{W}^L, \mathbf{E}^L, \mathbf{W}_y, \mathbf{E}_y\}$ . Each error filter/kernel is the same shape as its corresponding convolutional filter, i.e.,  $\mathbf{E}^\ell \in \mathcal{R}^{N_\ell \times N_{\ell-1} \times h_\ell \times w_\ell}$  (except  $\mathbf{E}_y$ , which is the same shapes as the transpose of  $\mathbf{W}_y$ ).

Assuming the tensor target activity  $\mathbf{y}^\ell$  is available to layer  $\ell$ , we compute each channel’s error neuron map as  $\mathbf{e}_{m, :, :}^\ell = -(\mathbf{y}_{m, :, :}^\ell - \mathbf{z}_{m, :, :}^\ell)$ . Using this mismatch signal, we then work our way down to layer  $\ell - 1$  by first convolving this error neuron map to project it downwards, using the appropriate error kernel. Once the projection is complete, if pooling has been applied to the output of each convolutional layer, we then up-sample the projection before computing the final target. This process proceeds formally as follows:

$$\mathbf{e}_{m, :, :}^\ell = -(\mathbf{y}_{m, :, :}^\ell - \mathbf{z}_{m, :, :}^\ell) \quad (3)$$

$$\mathbf{d}_{n, :, :}^{\ell-1} \leftarrow \mathbf{d}_{n, :, :}^{\ell-1} + \mathbf{E}_{m, n, :, :}^\ell \odot \mathbf{e}_{m, :, :}^\ell, \forall m \in N_\ell \quad (4)$$

$$\mathbf{d}_{n, :, :}^{\ell-1} \leftarrow \Phi_{up}(\mathbf{d}_{n, :, :}^{\ell-1}) \quad // \text{If max-pooling used} \quad (5)$$

$$\mathbf{y}_{n, :, :}^{\ell-1} = \phi^{\ell-1}(\mathbf{h}_{n, :, :}^{\ell-1} - \beta \mathbf{d}_{n, :, :}^{\ell-1}) \quad (6)$$

where we see that  $\Phi_{up}()$  denotes the up-sampling operation (to recover the dimensionality of the map before max-pooling was applied). Note that if pooling was not used in layer  $\ell - 1$ , then Equation 5 is omitted in the calculation of layer  $\ell - 1$ ’s target activity. Note that the update rule has a recursive nature, since it requires the existence of  $\mathbf{y}^\ell$  which in turn would have been created by applying Equations 3-6 to the layer above,  $\ell + 1$ . Thus, the base case target activity  $\mathbf{y}^L$ , which would exist at the very top (or highest level) of the CNN, and, in the case of supervised classification, which is the focus of this paper, this would be the target label vector  $\mathbf{y}$  associated with input image  $\mathbf{x}$ .

---

**Algorithm 1** EKDAA applied to a CNN w/ max-pooling and a fully-connected maximum entropy output.

---

```

Input: sample  $(\mathbf{y}, \mathbf{x})$ ,  $\beta$ , &  $\Theta$ 
// Feedforward inference
function INFER( $\mathbf{x}, \Theta$ )
    // Pass data thru convolution stack
    // Get image input channels
     $\mathbf{z}_{n,:,:}^0 = \mathbf{x}_{n,:,:}, \forall n \in N_0$ 
    for  $\ell = 1$  to  $L_C$  do
        // Calculate feature maps for layer  $\ell$ 
         $\mathbf{h}_{m,:,:}^\ell = \mathbf{0}, \forall m \in N_\ell$ 
        for  $m = 1$  to  $N_\ell$  do
             $\mathbf{h}_{m,:,:}^\ell \leftarrow \mathbf{h}_{m,:,:}^\ell + \mathbf{W}_{m,n,:,:}^\ell * \mathbf{z}_{n,:,:}^{\ell-1}, \forall n$ 
             $\mathbf{z}_{m,:,:}^\ell = \phi^\ell(\mathbf{h}_{m,:,:}^\ell),$ 
             $\mathbf{z}_{m,:,:}^\ell \leftarrow \Phi_{mp}(\mathbf{z}_{m,:,:}^\ell)$ 
         $\mathbf{h}_y = \mathbf{W}_y \cdot \text{Flatten}(\mathbf{z}^{L_C}), \mathbf{z}_y = \sigma(\mathbf{h}_y)$ 
         $\Lambda = \{(\mathbf{h}^1, \dots, \mathbf{h}^{L_C}, \mathbf{h}_y), (\mathbf{z}^0, \dots, \mathbf{z}^{L_C}, \mathbf{z}_y)\}$ 
    Return  $\Lambda$ 

    // Calculate weight updates via EKDAA
    function CALCUPDATES( $\Lambda, \mathbf{y}, \Theta$ )
         $\mathbf{h}^1, \dots, \mathbf{h}^{L_C}, \mathbf{h}_y, \mathbf{z}^0, \dots, \mathbf{z}^{L_C}, \mathbf{z}_y \leftarrow \Lambda, \mathbf{y}^L = \mathbf{y}$ 
        // Compute softmax weight updates
         $\mathbf{e}_y = -(\mathbf{y} - \mathbf{z}_y)$ 
         $\Delta \mathbf{W}_y = \mathbf{e}_y \cdot (\text{Flatten}(\mathbf{z}^{L_C}))^T,$ 
         $\Delta \mathbf{E}_y = -\gamma(\Delta \mathbf{W}_y)^T$ 
         $\mathbf{y}^{L_C} = \phi^{L_C}(\text{Flatten}(\mathbf{h}^{L_C}) - \beta(\mathbf{E} \cdot \mathbf{e}_y))$ 
        // Compute convolutional kernel updates
         $\mathbf{y}^{L_C} \leftarrow \text{UnFlatten}(\mathbf{y}^{L_C})$ 
        for  $\ell = L_C$  to 1 do
            for  $m = 1$  to  $N_\ell$  do
                 $\mathbf{e}_{m,:,:}^\ell = -(\mathbf{y}_{m,:,:}^\ell - \mathbf{z}_{m,:,:}^\ell)$ 
             $\mathbf{d}^\ell = \mathbf{0}, \forall n \in N_{\ell-1}$ 
            for  $n = 1$  to  $N_{\ell-1}$  do
                for  $m = 1$  to  $N_\ell$  do
                     $\mathbf{d}_{n,:,:}^{\ell-1} \leftarrow \mathbf{d}_{n,:,:}^{\ell-1} +$ 
                     $(\mathbf{E}_{m,n,:,:}^\ell \odot \mathbf{e}_{m,:,:}^\ell)$ 
                 $\mathbf{y}_{n,:,:}^{\ell-1} = \phi^{\ell-1}(\mathbf{h}_{n,:,:}^{\ell-1} - \beta \Phi_{up}(\mathbf{d}_{n,:,:}^{\ell-1}))$ 
            for  $m = 1$  to  $N_\ell$  do
                for  $n = 1$  to  $N_{\ell-1}$  do
                     $\Delta \mathbf{W}_{m,n,:,:}^\ell = \mathbf{z}_{n,:,:}^{\ell-1} * \text{Flip}(\mathbf{e}_{m,:,:}^\ell)$ 
                     $\Delta \mathbf{E}_{m,n,:,:}^\ell = -\gamma(\Delta \mathbf{W}_{m,n,:,:}^\ell)^T$ 
             $\Delta = \{\Delta \mathbf{W}^0, \Delta \mathbf{E}^0, \dots, \mathbf{W}^{L_C}, \Delta \mathbf{E}^{L_C}, \mathbf{W}_y, \mathbf{E}_y\}$ 
    Return  $\Delta$ 

```

---

Once targets have been computed for each convolutional layer, the adjustment for each filter/kernel in each requires a specialized local rule that entails convolving the post-activation maps of the level below with the error neuron map at  $\ell$ . Formally, this means:

$$\Delta \mathbf{W}_{m,n,:,:}^\ell = \mathbf{z}_{n,:,:}^{\ell-1} * \text{Flip}(\mathbf{e}_{m,:,:}^\ell) \quad (7)$$

$$\Delta \mathbf{E}_{m,n,:,:}^\ell = -\gamma(\Delta \mathbf{W}_{m,n,:,:}^\ell)^T \quad (8)$$

which can then subsequently be treated as the gradient to be used in either a stochastic gradient descent update, i.e.,  $\mathbf{W}_{m,n,:,:}^\ell \leftarrow \mathbf{W}_{m,n,:,:}^\ell - \lambda \Delta \mathbf{W}_{m,n,:,:}^\ell$ , or a more advanced rule such as Adam [25] or RMSprop [26].

In Algorithm 1, we provided a full mathematical description of how EKDAA would be applied to a deep CNN specialized for classification. Note that while this paper focuses on feedforward classification, our approach is not dependent on the type of task that the CNN is required to solve. For example, one could readily employ our approach to learn convolutional autoencoders for the case of unsupervised learning.

One key advantage of the above approach is that the test-time inference of the CNN that is learned with the proposed EKDAA is no slower than a standard backprop-trained CNN since the forward pass here remains the same. Note that, while the above error neuron map, target activity, and kernel updates are presented in an individual per-channel/filter form (a naïve implementation would involve a for-loop that iterated over every single filter/feature map in a layer), our concrete implementation of the equations above involved the more efficient Toeplitz matrix form, to better exploit the computational power afforded by GPU hardware.

## 4 Experimental Setup and Results

### 4.1 Datasets and Experimental Tasks

To understand learning capacity for fitting and generalization under EKDAA, we design and train several models and test them against three standard datasets. Specifically, we evaluated on Fashion MNIST [27] (FMNIST), CIFAR-10 [28], and SVHN [29].

Fashion MNIST, while only being a single channel (gray-scale) image dataset at a  $[28 \times 28]$  resolution, has a more complicated pixel input space than MNIST, facilitating a better analysis of the convolutional contribution to overall network performance. Furthermore, we utilized t-SNE to visualize the outputs from the topmost convolutional layer across epochs in order to see how EKDAE disentangles the feature space of Fashion MNIST. CIFAR-10 and SVHN, on the other hand, are used to test how EKDAE operates on real-life natural color images.

Taken together, the FMNIST, CIFAR-10, and SVHN datasets allow us to investigate not only how well EKDAE learns filters when engaged in the process of data fitting but also how effective it is in creating models that generalize on visual datasets. Additionally, we show that our networks can be trained using non-differentiable activations, such as the signum function, or, more formally:  $\text{signum}(x) = 1$  if  $x > 0$ ,  $0$  if  $x = 0$ ,  $-1$  if  $x < 0$ . In this case, we train all convolutional and fully-connected layers of our model using signum as the activation function, except for the softmax output layer, in order to investigate how well an EKDAE-driven network handles non-differentiable activity without any specific tuning.

## 4.2 Technical Implementation

We design convolutional neural networks for the Fashion MNIST, CIFAR-10, and SVHN datasets. The Fashion MNIST CNN consists of three convolutional layers before flattening and propagating through one fully-connected layer followed by a softmax. The filter size is  $[3 \times 3]$  for all convolutional layers with the first layer starting with one channel, expanding to 32 to 64 and finishing at 128 filters. The fully connected layers start after flattening the filters which are then propagated through 128 fully-connected nodes before finishing at 10 output nodes (one per image class). Max-pooling with a kernel of  $[2 \times 2]$  and a stride of 2 was used at the end of the first and second layers of convolution.

The CIFAR-10 and SVHN models use six layers of convolution and is inspired by the blocks of convolution and pooling layers used in the VGG family of networks [30]. First, two convolutional layers are used before finally passing through a max-pooling layer with a kernel of  $[2 \times 2]$  and a stride of two. Three of these mini-blocks of two convolution layers, followed by a max-pooling layer, are used to build the final network. The first three layers of convolution use 64 filters while the last three layers use 128 filters. All layers use a filter size of  $[3 \times 3]$ . After traversing through the last convolutional layer, the final neural activities are flattened and propagated through a single 128-node, fully-connected layer before shrinking down to 10 output nodes (which are run through the softmax nonlinearity). Both Fashion MNIST, SVHN, and CIFAR-10 models use a very small amount of fully-connected nodes and instead use multiple large filter layers to learn/extract distributed representations (see Appendix for details).

Each model was tuned for optimal performance and several hyper-parameters were adjusted including: batch size, learning rate, filter size, number of filters per layer, number of fully-connected nodes per layer, weight initialization, optimizer choice, and dropout rate. Additional details can be found in Appendix. This exact architecture was used for the EKDAE model as well as for the other learning mechanisms that it was compared against. Models were optimized using stochastic gradient descent with momentum and Pascanu re-scaling was applied to all layer-wise weight updates.

All models were trained on the original datasets at the original image resolutions without any data augmentation or pre-training. Unlike backprop, EKDAE did not benefit from extensive heuristic knowledge as to what optimal parameterization would look like, making a grid search for parameters ineffective as the tuning limits would be significantly wider than with backprop. As a result, for tuning, the learning rate was tuned from the range  $1e-1$  to  $1e-4$ , number of filters were tuned from the range 32 to 128, dropout was tuned from 0 to 0.5, and the activation function was evaluated to be either the hyperbolic tangent (tanh) or the linear rectifier (relu). The final meta-parameter setting for EKDAE was a learning rate of  $0.5e-3$ , 0.9 momentum rate, tanh for activation, and a dropout rate of 0.1 for filters and 0.3 for fully-connected layers (complete model specifications are in the Appendix). All model weights were randomly initialized with system time as a seed. Furthermore, all models were trained on a single Tesla P4 GPU with 8GB of GPU RAM and ran on Linux Ubuntu 18.04.5 LTS, using Tensorflow 2.1.0. The code for this work has been designed in a novel library that allows for defining convolutional and fully-connected models with the ability to quickly change the learning mechanism between BP and EKDAE. The library also allows for defining new custom learning rules for analysis. While this codebase offers a powerful advantage for analyzing learning mechanisms, it has been custom written without the optimization techniques that common libraries have implemented. This codebase takes advantage of Tensorflow tensors when possible but has a custom defined forward and backward pass that is not nearly as memory or computationally efficient as it can be.

	FMNIST		SVHN		CIFAR-10	
	Train Acc	Test Acc	Train Acc	Test Acc	Train Acc	Test Acc
BP	95.31 $\pm$ 0.18	89.97 $\pm$ 0.14	90.98 $\pm$ 0.23	88.52 $\pm$ 0.10	83.33 $\pm$ 0.22	71.08 $\pm$ 0.08
BP (FC)	92.91 $\pm$ 0.39	87.02 $\pm$ 0.41	84.36 $\pm$ 0.12	79.81 $\pm$ 0.22	57.05 $\pm$ 0.34	55.03 $\pm$ 0.29
LRA-E (FC)	93.59 $\pm$ 0.26	87.58 $\pm$ 0.33	80.17 $\pm$ 0.08	73.24 $\pm$ 0.19	58.10 $\pm$ 0.28	55.51 $\pm$ 0.42
EKDA	95.83 $\pm$ 0.33	90.01 $\pm$ 0.11	84.31 $\pm$ 0.21	82.27 $\pm$ 0.19	75.05 $\pm$ 0.27	63.38 $\pm$ 0.12
EKDA, Sig. HSIC [11]	94.00 $\pm$ 0.14	88.69 $\pm$ 0.06	79.43 $\pm$ 0.09	76.87 $\pm$ 0.13	64.22 $\pm$ 0.12	59.71 $\pm$ 0.08
FA	95.30 $\pm$ 0.51	89.10 $\pm$ 0.18	79.18 $\pm$ 0.22	76.50 $\pm$ 0.18	77.50 $\pm$ 0.25	58.80 $\pm$ 0.11
DFA	93.99 $\pm$ 0.32	88.90 $\pm$ 0.10	82.50 $\pm$ 0.24	80.30 $\pm$ 0.21	79.50 $\pm$ 0.20	60.50 $\pm$ 0.08
SDFA	94.10 $\pm$ 0.28	89.00 $\pm$ 0.10	84.50 $\pm$ 0.23	81.40 $\pm$ 0.19	80.00 $\pm$ 0.19	59.60 $\pm$ 0.06
DRTP	93.50 $\pm$ 0.40	87.99 $\pm$ 0.15	85.21 $\pm$ 0.21	81.90 $\pm$ 0.20	79.50 $\pm$ 0.22	58.20 $\pm$ 0.14

Table 1: Train and test accuracy on the Fashion MNIST, SVHN, and CIFAR-10 datasets. Mean and standard deviation over 10 trials reported. It is important to note here that the signum (sig.) function is included only to demonstrate that we are able to successfully train a non-differentiable activation function using EKDA, and obtain reasonable performance. FC stands for fully-connected.

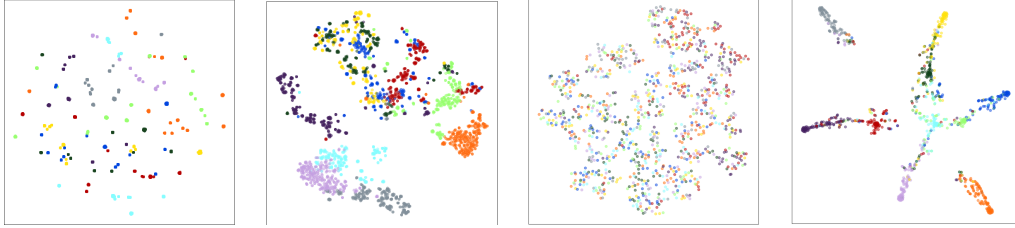


Figure 2: t-SNE visualization depicting the learned representations of EKDA, shown for Epoch 0 (initial weights) and the final training epoch: (Left:) FMNIST and (Right) CIFAR-10.

#### 4.3 EKDA Robustness Analysis

**Fast-Gradient Sign Method Attack:** In [31], the Fast-Gradient Sign Method (FGSM) was proposed as a way to quickly generate adversarial examples for convolutional models. FGSM (as shown in Equation 9) applies noise that is generated from the opposite direction of the gradients of the network’s optimization trajectory, ultimately trying to maximize the distance between the predicted and ground truth label for images. In addition, restrictions are put on the adversarial image as to not modify the original input beyond a set threshold, enforcing that the generated images look visually similar and indistinguishable to humans. FGSM is formally defined as:

$$\mathbf{x}_{adv} = \mathbf{x} + \epsilon * \text{signum}(\nabla_x J(\Theta, \mathbf{x}, \mathbf{y})) \quad (9)$$

where  $\mathbf{x}_{adv}$  is the adversarial image of the original input  $\mathbf{x}$  that has the label  $\mathbf{y}$ . The loss function  $J$  is used in conjunction with the model parameters  $\Theta$  and has the adversarial noise limited/controlled by  $\epsilon$ .

**Carlini and Wagner (C&W) Attack:** [32] (C&W) proposed a more robust adversarial attack as depicted in Equation 10, with the best found objective presented in Equation 11, to generate adversarial images. While the C&W approach takes longer to generate samples, it provides stronger adversarial attack images and provides a benchmark standard for defense systems. Formally, C&W is:

$$\begin{aligned} \text{minimize : } & \|\delta\|_p + c * f(\mathbf{x} + \delta) \\ \text{such that : } & \mathbf{x} + \delta \in [0, 1]^n \end{aligned} \quad (10)$$

where the objective function  $f$  uses the input  $\mathbf{x}$  and distance metric  $\delta$ , controlled by a threshold  $c$ . The objective function itself is defined formally as follows:

$$f(\mathbf{x}') = \max(\max\{Z(\mathbf{x}')_i : i \neq t\} - Z(\mathbf{x}')_t, -k) \quad (11)$$

where an adversarial image,  $\mathbf{x}'$ , is generated using the input image label,  $i$  along with a target,  $t$ , while staying within the constraint of  $k$  to generate realistic attack samples (see Figure 3 for samples).

The C&W attack (see Figure 3 for samples) makes use of a distance metric to quantify the similarity between the input image and generated adversarial image. The distance metric takes the form of the  $l_p$  norm. There are three distance metrics that [32] propose for the attack.  $l_0$  distance calculates the number of pixels such that  $\mathbf{x}_i \neq \mathbf{x}'_i$ .  $l_2$  distance calculates the Euclidean distance between  $\mathbf{x}_i$  and  $\mathbf{x}'_i$ .  $l_\infty$  (the infinity norm) distance calculates the maximum change to the pixel in  $\mathbf{x}'_i$ .

## Black Box Robustness Experiments

In real-world scenarios, adversarial attacks are attempted on neural models that are deployed and actively in use. The adversary has no access to the deployed model or its specifications. Notably, this style of black box attack requires the use of a proxy model for approximating the target model to be attacked. We opted to test adversarial robustness by applying two black box attacks by employing both FGSM as well as C&W for all datasets. To serve as a proxy model, a four layer convolutional network is used with the first two layers having 32 filters, and the last two convolutional layers having two 64 filters. Max pooling is applied after the second and forth convolutional layers and is then concatenated and fed into a fully connected layer of 128 nodes and a final output layer of 10 nodes with a softmax activation applied. This model configuration is different from the originally trained models in order to function as an unknown proxy model in our tests. In Table 2, we see that, desirably, EKDA offers some protection/robustness against FGSM and C&W in contrast to backprop, quite notably on the Fashion MNIST dataset.

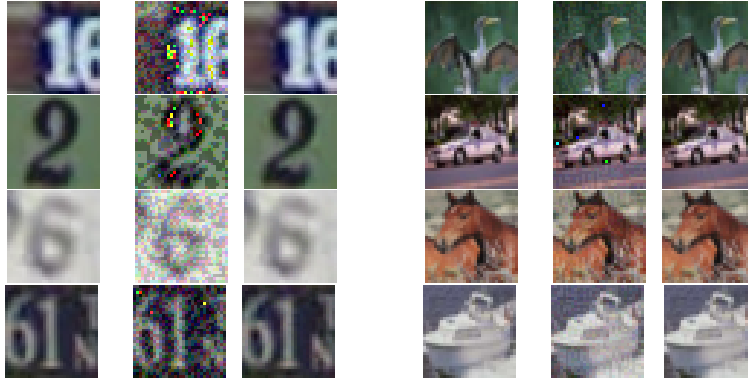


Figure 3: Adversarial image examples for the SVHN (Left group) and CIFAR-10 (right group) datasets. Original images (left) have the fast gradient sign method attack (middle), as well as the Carnili & Wagner attack (Right) applied to them.

Learning Algorithm	Attack Method	FMNIST	SVHN	CIFAR10
BP	FGSM $\epsilon = 0.10$	24.66	14.20	40.50
EKDA	FSGM $\epsilon = 0.10$	49.84	18.70	44.10
BP	C&W	40.20	18.40	10.50
EKDA	C&W	83.86	19.00	13.00

Table 2: Adversarial robustness analysis of the fast gradient sign method and Carlini and Wagner attack applied to BP and EKDA trained networks. 1000 images from the Fashion MNIST, SVHN, and CIFAR-10 test sets are used to analyze the accuracy of the models against the foolable/adversarial images.

### 4.4 Discussion

We analyzed EKDA by comparing it to both backprop (BP) as well as HSIC [11], RFA [14], DFA [16], sparse direct feedback alignment (SDFA) [18], and direct random target projection (DRTP) [33] (see Appendix for baseline details). The results are presented in Table 1 (we also added two fully-connected baselines – an MLP trained by backprop and one trained by LRA-E [9]). We find that EKDA performs competitively with all other algorithms and exhibits both training and test accuracy more similar to that of backprop. Additionally, when testing EKDA with the signum activation, we find that the resulting CNN is able to operate with the non-differentiable function successfully on Fashion MNIST. Notably, on CIFAR-10 (as well as on SVHN and Fashion MNIST), we find that EKDA outperforms all of the other BP-free methods tested.

Figure 2 shows the t-SNE plots for a Fashion MNIST and CIFAR-10 CNN trained with EKDA. The t-SNE plots were generated (at the 0th and 40th epoch) and visualized using default t-SNE parameters (i.e. no tuning) with a perplexity value of 30 and the maximum number of iterations set to 1000. Qualitatively, we find that the EKDA learning process successfully learns to group features together with only the convolutional layers, indicating that the error kernels learned are indeed benefiting the CNN model.

While many biologically-plausible alternatives have also been developed to learn models of natural images, many of them incorporate the computation of error derivatives as part of the process and the architectures that

they are generally applied to have been designed with multiple, large fully-connected layers with only a few convolutional layers. We argue that adding many fully connected layers corrupts the original input signal such that the neural model is engaged in a greedy optimization process that results in fitting to noise rather than extracting useful features from natural image inputs. Therefore, the role of convolution in such models is still debatable and, as a result, it is difficult to determine if model generalization/performance is coming from the bio-plausible learning mechanism or from the fully-connected layers. In contrast, EKDA emphasizes the role of convolutional filters in extracting useful image features while reducing the amount of fully-connected elements. Our results on the three datasets examined above validate that this approach still yields models that generalize well. We believe that the models learned with this focus in mind can result in CNN models that acquire robust distributed representations that are capable of dealing with corrupt or even adversarial samples, as evidenced by our promising analysis results shown in Table 2.

**Limitations:** The main limitation of the proposed EKDA algorithm is currently related to its scalability to massive datasets, especially when compared with highly optimized tensor computations that are implemented in standard deep learning libraries that support backprop-based convolution/deconvolution operations. Currently, EKDA would not scale easily to networks with many layers or more than several hundred filters without optimization of its filter operations. Our primary future work will be to modularize the current state of EKDA code to improve its ability to scale to large datasets, e.g., ImageNet [34]. Due to the current lack of optimization compared to frameworks like TensorFlow and PyTorch, the proposed framework is not currently as efficient requiring more computational resources than the more established frameworks. In the Appendix, we provide further discussion of limitations. One possible consequence of constructing more effective backprop-free alternatives to convolutional models would be the improvement of performance of the computational intelligence that drives systems such as drones, which would result in the loss of life. In the Appendix, we provide an expanded discussion of the negative societal impact of our work.

## 5 Conclusion

We have presented an initial exploration of a back-propagation (backprop)-free convolutional neural network learning algorithm. We implemented a local feedback mechanism that transmits information across layers in order to compute target activity values and relevant error neuron maps (independent of activation function type), resulting in Hebbian-like update rules for the convolutional filters of a CNN. Specifically, this credit assignment process was made possible through the introduction of a mechanism that we call the error kernel, which provides a means to reverse filter error neuron activity signals and complements the normal filters used to extract features in convolutional models. We refer to our proposed process as the *error-kernel driven activation alignment (EKDA)* method. In this work, we compared various learning algorithms in training a small CNN. We find that EKDA obtains similar performance compared to standard learning techniques such as backprop and also outperforms other bio-inspired alternatives. Notably, our method offers several benefits. It resolves the weight transport problem, works with non-differentiable activities, and is computationally efficient since it can operate in a layer-wise parallel/asynchronous fashion.

Our experiments demonstrated that EKDA learns “good” representations during training and, furthermore, we found that an EKDA-trained CNN acquires latent representations that improve over time (epochs) as training evolves. In addition, we show that EKDA provides increased, more natural robustness to common gradient-based adversarial attacks including the fast-gradient sign method and Carnili & Wagner attack. While there is still much to explore in future work, we have successfully presented an analysis of the novel EKDA algorithm, yielding promising evidence that it is capable of training convolutional networks without backprop. The implication of this could have far-reaching effects in expanding the future designs of CNN architectures.

## References

- [1] H. Markram and B. Sakmann, “Action potentials propagating back into dendrites trigger changes in efficacy of single-axon synapses between layer v pyramidal neurons,” in *Soc. Neurosci. Abstr.*, vol. 21, no. 3, 1995, p. 2007.
- [2] D. O. Hebb, “The organization of behavior; a neuropsychological theory,” *A Wiley Book in Clinical Psychology*, vol. 62, p. 78, 1949.
- [3] T. C. Südhof and R. C. Malenka, “Understanding synapses: past, present, and future,” *Neuron*, vol. 60, no. 3, pp. 469–476, 2008.
- [4] F. Crick, “The recent excitement about neural networks,” *Nature*, vol. 337, no. 6203, pp. 129–132, 1989.
- [5] T. P. Lillicrap, A. Santoro, L. Marris, C. J. Akerman, and G. Hinton, “Backpropagation and the brain,” *Nature Reviews Neuroscience*, vol. 21, no. 6, pp. 335–346, 2020.

[6] K. He, X. Zhang, S. Ren, and J. Sun, “Deep residual learning for image recognition,” in *Proceedings of the IEEE conference on computer vision and pattern recognition*, 2016, pp. 770–778.

[7] V. Mnih, K. Kavukcuoglu, D. Silver, A. Graves, I. Antonoglou, D. Wierstra, and M. Riedmiller, “Playing atari with deep reinforcement learning,” *arXiv preprint arXiv:1312.5602*, 2013.

[8] R. Pascanu, T. Mikolov, and Y. Bengio, “On the difficulty of training recurrent neural networks,” in *International conference on machine learning*. PMLR, 2013, pp. 1310–1318.

[9] A. G. Ororbia and A. Mali, “Biologically motivated algorithms for propagating local target representations,” in *Proceedings of the AAAI Conference on Artificial Intelligence*, vol. 33, 2019, pp. 4651–4658.

[10] M. Minsky, “Steps toward artificial intelligence,” *Proceedings of the IRE*, vol. 49, no. 1, pp. 8–30, 1961.

[11] W.-D. K. Ma, J. P. Lewis, and W. B. Kleijn, “The hsic bottleneck: Deep learning without back-propagation,” 2019.

[12] N. Tishby, F. C. Pereira, and W. Bialek, “The information bottleneck method,” *arXiv preprint physics/0004057*, 2000.

[13] T. Salimans, J. Ho, X. Chen, S. Sidor, and I. Sutskever, “Evolution strategies as a scalable alternative to reinforcement learning,” *arXiv preprint arXiv:1703.03864*, 2017.

[14] T. Lillicrap, D. Cownden, D. Tweed, and C. Akerman, “Random synaptic feedback weights support error backpropagation for deep learning,” *Nature Communications*, vol. 7, no. 13276, pp. 1–10, 2016.

[15] S. Grossberg, “Competitive learning: From interactive activation to adaptive resonance,” *Cognitive Science*, vol. 11, no. 1, pp. 23–63, 1987. [Online]. Available: <https://onlinelibrary.wiley.com/doi/abs/10.1111/j.1551-6708.1987.tb00862.x>

[16] A. Nøkland, “Direct feedback alignment provides learning in deep neural networks,” 2016.

[17] D. Han, G. Park, J. Ryu, and H.-j. Yoo, “Extension of direct feedback alignment to convolutional and recurrent neural network for bio-plausible deep learning,” *arXiv preprint arXiv:2006.12830*, 2020.

[18] B. Crafton, A. Parihar, E. Gebhardt, and A. Raychowdhury, “Direct feedback alignment with sparse connections for local learning,” *Frontiers in neuroscience*, vol. 13, p. 525, 2019.

[19] T. Chu, K. Mykityuk, M. Szewczyk, A. Wiktor, and Z. Wojna, “Training dnns in  $O(1)$  memory with mem-dfa using random matrices,” *arXiv preprint arXiv:2012.11745*, 2020.

[20] D.-H. Lee, S. Zhang, A. Fischer, and Y. Bengio, “Difference target propagation,” 2015.

[21] S. Bartunov, A. Santoro, B. Richards, L. Marrs, G. E. Hinton, and T. Lillicrap, “Assessing the scalability of biologically-motivated deep learning algorithms and architectures,” in *Advances in Neural Information Processing Systems*, 2018, pp. 9368–9378.

[22] A. G. Ororbia, A. Mali, D. Kifer, and C. L. Giles, “Conducting credit assignment by aligning local representations,” 2018.

[23] A. Ororbia, A. Mali, D. Kifer, and C. L. Giles, “Reducing the computational burden of deep learning with recursive local representation alignment,” *arXiv preprint arXiv:2002.03911*, 2020.

[24] A. Clark, *Surfing uncertainty: Prediction, action, and the embodied mind*. Oxford University Press, 2015.

[25] D. P. Kingma and J. Ba, “Adam: A method for stochastic optimization,” 2017.

[26] T. Tieleman and G. Hinton, “Lecture 6.5—RmsProp: Divide the gradient by a running average of its recent magnitude,” COURSERA: Neural Networks for Machine Learning, 2012.

[27] H. Xiao, K. Rasul, and R. Vollgraf, “Fashion-mnist: a novel image dataset for benchmarking machine learning algorithms,” 2017.

[28] A. Krizhevsky, V. Nair, and G. Hinton, “The cifar-10 dataset,” *online*: <http://www.cs.toronto.edu/kriz/cifar.html>, vol. 55, 2014.

[29] Y. Netzer, T. Wang, A. Coates, A. Bissacco, B. Wu, and A. Y. Ng, “Reading digits in natural images with unsupervised feature learning,” in *NIPS Workshop on Deep Learning and Unsupervised Feature Learning 2011*, 2011. [Online]. Available: [http://ufldl.stanford.edu/housenumbers/nips2011\\_housenumbers.pdf](http://ufldl.stanford.edu/housenumbers/nips2011_housenumbers.pdf)

[30] K. Simonyan and A. Zisserman, “Very deep convolutional networks for large-scale image recognition,” *arXiv preprint arXiv:1409.1556*, 2014.

[31] I. J. Goodfellow, J. Shlens, and C. Szegedy, “Explaining and harnessing adversarial examples,” 2015.

[32] N. Carlini and D. A. Wagner, “Towards evaluating the robustness of neural networks,” *CoRR*, vol. abs/1608.04644, 2016. [Online]. Available: <http://arxiv.org/abs/1608.04644>

[33] C. Frenkel, M. Lefebvre, and D. Bol, “Learning without feedback: Fixed random learning signals allow for feedforward training of deep neural networks,” *Frontiers in Neuroscience*, vol. 15, p. 20, 2021.

[34] J. Deng, W. Dong, R. Socher, L.-J. Li, K. Li, and L. Fei-Fei, “Imagenet: A large-scale hierarchical image database,” in *2009 IEEE conference on computer vision and pattern recognition*. IEEE, 2009, pp. 248–255.

[35] M. Akrout, C. Wilson, P. C. Humphreys, T. Lillicrap, and D. Tweed, “Deep learning without weight transport,” *arXiv preprint arXiv:1904.05391*, 2019.

[36] A. Nøkland and L. H. Eidnes, “Training neural networks with local error signals,” in *International Conference on Machine Learning*. PMLR, 2019, pp. 4839–4850.

[37] L. Grinberg, J. Hopfield, and D. Krotov, “Local unsupervised learning for image analysis,” *arXiv preprint arXiv:1908.08993*, 2019.

[38] J. Guerguiev, T. P. Lillicrap, and B. A. Richards, “Towards deep learning with segregated dendrites,” *Elife*, vol. 6, p. e22901, 2017.

[39] J. Schmidhuber, “Networks adjusting networks,” in *Proceedings of Distributed Adaptive Neural Information Processing*, 1990, pp. 197–208.

[40] P. J. Werbos, “Applications of advances in nonlinear sensitivity analysis,” in *System modeling and optimization*. Springer, 1982, pp. 762–770.

[41] S. Linnainmaa, “The representation of the cumulative rounding error of an algorithm as a taylor expansion of the local rounding errors,” *Master’s Thesis (in Finnish)*, Univ. Helsinki, pp. 6–7, 1970.

[42] W. Xiao, H. Chen, Q. Liao, and T. Poggio, “Biologically-plausible learning algorithms can scale to large datasets,” *arXiv preprint arXiv:1811.03567*, 2018.

[43] B. Lansdell, P. Prakash, and K. Kording, “Learning to solve the credit assignment problem,” *arXiv preprint arXiv:1906.00889*, 2019.

[44] M. Jaderberg, W. M. Czarnecki, S. Osindero, O. Vinyals, A. Graves, D. Silver, and K. Kavukcuoglu, “Decoupled neural interfaces using synthetic gradients,” in *International Conference on Machine Learning*. PMLR, 2017, pp. 1627–1635.

[45] P. Henderson, J. Hu, J. Romoff, E. Brunskill, D. Jurafsky, and J. Pineau, “Towards the systematic reporting of the energy and carbon footprints of machine learning,” *Journal of Machine Learning Research*, vol. 21, no. 248, pp. 1–43, 2020.

## Appendix

### A Extended Related Works

In addition to related Hebbian learning rules, other related work includes alternative convolution-based learning schemes such as those found in [35] that base their work on the Kollen-Pollack (KP) method and have demonstrated promising results on larger, more extensive benchmarks. Other training approaches are based on local losses [36, 37, 38, 39, 40, 41]; are methods that take the sign of the forward activities [42]; are schemes that utilize noise-based feedback modulation [43]; or use synthetic gradients [44] to stabilize learning for deeper networks. These approaches have shown better or comparable performance (to backprop) on challenging benchmarks using the convolution operator. However, there are significant dependencies on the network model’s forward activities used to guide the backward signal propagation, hence, these approaches belong to a different class of problems/algorithms than what we address in this work.

### B Experimental Setup Details

We performed a grid search for all of the models investigated in this work in order to find optimal meta-parameters and extract optimal behavior for each. Primarily, tuned hyper-parameters included: batch size, learning rate, filter size, number of filters per layer, number of fully-connected nodes/units per layer, weight initialization, choice of optimizer, and the dropout rate. Note that this work does not aim to obtain state-of-the-art image classification results. Rather, its intent is to present a method that efficiently tackles the credit assignment issues in a convolution neural network (CNN) by effectively operating with our proposed error kernel mechanism. Furthermore, our method offers additional flexibility in design choices (such as permitting the use of non-differentiable activation functions).

**Meta-parameter Tuning:** We report our grid search ranges for each model’s meta-parameters in Tables 1 (EKDA), 6 (DFA), 5 (FA), 8 (RDFA), and 7 (SDFA), respectively. Furthermore, in the “Best” column, we report the final values selected/used for the models reported in the main paper.

**Architecture Design:** In Table 3, we present the architectures used across the learning algorithms investigated in this paper, i.e., the proposed EKDA, feedback alignment (FA, also referred to as RFA in the main paper), direct feedback alignment (DFA), sparse direct feedback alignment (SDFA), and random direct feedback alignment (RDFA). We built the models for Fashion MNIST, SVHN, and CIFAR-10 to include several layers of convolution (conv), with a sizeable amount of filters, and only small (in terms of dimensionality) fully-connected (fc) layers to focus the learning process on adapting/using the model kernels/filters to extract useful features from the input image signals. In particular, the model for SVHN and CIFAR-10 had multiple layers with 128 filters per layer and, before flattening the activities for the

fully-connected layers, the image size was reduced using three max pooling layers in order to propagate forward the image to obtain a  $[4 \times 4]$  resolution.

**General Comments/Discussion:** With respect to the main paper’s results, what is significant about our findings is that EKDA demonstrates that adjusting the synaptic weight parameters of a CNN is possible using recurrent error synapses formulated as error kernels themselves. This means that the target feature map values (and the error neuron maps that calculate the distance between the original feature maps and these targets) inherent to our backprop-free computational process provide useful teaching signals that facilitate the learning of useful neural vision architectures. The main results of our paper provide promising initial evidence that EKDA can serve as a potentially useful bio-inspired alternative to backprop for training CNNs on natural images.

## C On Limitations and Potential Negative Societal Impact

The primary limitation of our proposed EKDA algorithm is currently its ability to scale, particularly when compared to the highly optimized tensor computations implemented in standard deep learning libraries that provide direct support for backprop-based convolution/deconvolution operations. Currently, based on our practical experience with our custom software library that implements EKDA, it appeared to us that EKDA does not scale easily to very large networks with many filters in each layer given a constrained computational budget and hardware (note that we were constrained in the amount of memory that we could allocate in a given GPU – at maximum, the GPUs available to us only facilitated a maximum of 8GB of workable memory, constraining the types of convolutional structures that we could ultimately explore). Specifically, we used one Ubuntu 18.04 server that had an 8GB Tesla P4, an Intel Xeon CPU E5-2650, and 256GB of RAM.

Our primary future work will be to further modularize the current state of our software library and its implementation of EKDA, focusing on engineering/extending it so as to improve the algorithm’s ability to scale to training on much larger datasets such as ImageNet.

While this area of work is promising, there are drawbacks when compared to using the well-studied and refined back-propagation learning algorithm. Currently, as mentioned before, our approach is not nearly as optimized for memory and GPU usage as compared to the back-propagation procedure that is implemented in popular frameworks such as TensorFlow or PyTorch, requiring more GPU resources and energy to run equivalent models of the more established frameworks.

Furthermore, modern deep learning based models running GPUs consume a high amount of energy [45]. Our proposed method, which also falls into the class of deep learning algorithms, has a significant carbon footprint which inadvertently has major potential climate impacts. As part of future work, we intend to run our algorithm through energy tracking tools [45] that can provide a detailed carbon impact summary generated by our framework.

## D Asset Usage

We build our codebase on top of TensorFlow 2.0 for fundamental functionality. TensorFlow is open-source with an Apache license. In addition, for analysis we use the publicly available FashionMNIST, SVHN, and CIFAR-10 datasets, all of which have licenses permitting unlimited use and modification. In addition, none of the datasets used in this study entail any data that could be considered sensitive (thus not requiring data consent) or offensive.

## E Model and Training Specifications

Layer	Fashion MNIST	Fashion MNIST Output	SVHN/CIFAR-10	SVHN/CIFAR-10 Output
L0	Input	[:, 28, 28, 1]	Input	[:, 32, 32, 3]
L1	Conv1 (1, 32) [3 x 3]	[:, 28, 28, 32]	Conv1 (3, 64) [3 x 3]	[:, 32, 32, 64]
L2	MaxP1 (2, 2)	[:, 14, 14, 32]	Conv2 (64, 64) [3 x 3]	[:, 32, 32, 64]
L3	Conv2 (32, 64) [3 x 3]	[:, 14, 14, 64]	MaxP1 (2, 2)	[:, 16, 16, 64]
L4	MaxP2 (2, 2)	[:, 7, 7, 64]	Conv3 (64, 64) [3 x 3]	[:, 16, 16, 64]
L5	Conv3 (64, 128) [3 x 3]	[:, 7, 7, 128]	Conv4 (64, 128) [3 x 3]	[:, 16, 16, 128]
L6	Flatten()	[:, 6272]	MaxP2 (2, 2)	[:, 8, 8, 128]
L7	FC1 (6272, 128)	[:, 128]	Conv5 (128, 128) [3 x 3]	[:, 8, 8, 128]
L8	Softmax (128, 10)	[:, 10]	Conv6 (128, 128) [3 x 3]	[:, 8, 8, 128]
L9	-	-	MaxP3 (2, 2)	[:, 4, 4, 128]
L10	-	-	Flatten()	[:, 2048]
L11	-	-	FC1 (2048, 128)	[:, 128]
L12	-	-	Softmax (128, 10)	[:, 10]

Table 3: Model architectures that were trained on Fashion MNIST, SVHN, and CIFAR-10. The layers of each model are defined as well as the outputs from each layer.

Parameter	Range Min	Range Max	Interval	Activation Functions	Best
batch_size	50	200	50	-	50
learning_rate	1e-5	1e-2	0.5	-	5e-4
filter_size	3	7	2	-	3
num_filters	32	256	32	-	-
fc_per_layer	128	128	-	-	128
weight_init	-	-	-	glorot_uniform, glorot_normal	glorot_uniform
optimizer	-	-	-	tanh, relu, signum	tanh
dropout	0.0	0.5	0.1	-	0.1 conv, 0.3 fc

Table 4: Hyper-parameter tuning ranges and best found parameters for EKDAA.

Parameter	Range Min	Range Max	Increment	Activation Functions	Best
batch_size	32	256	64	-	64
learning_rate	5e-5	3e-2	0.5	-	5e-4
filter_size	3	7	2	-	3
num_filters	32	256	32	-	-
fc_per_layer	128	128	-	-	128
weight_init	-	-	-	glorot_uniform, glorot_normal	glorot_normal
optimizer	-	-	-	tanh, relu	relu
dropout	0.0	0.5	0.1	-	0.1 conv, 0.3 fc

Table 5: Hyper-parameter tuning ranges and best found parameters for random feedback alignment (FA).

Parameter	Range Min	Range Max	Increment	Activation Functions	Best
batch_size	32	256	64	-	64
learning_rate	5e-5	3e-2	0.5	-	5e-3
filter_size	3	7	2	-	3
num_filters	32	256	32	-	-
fc_per_layer	128	128	-	-	128
weight_init	-	-	-	glorot_uniform, glorot_normal	glorot_uniform
optimizer	-	-	-	tanh, relu	relu
dropout	0.0	0.5	0.1	-	0.1 conv, 0.2 fc

Table 6: Hyper-parameter tuning ranges and best found parameters for direct feedback alignment (DFA).

Parameter	Range Min	Range Max	Increment	functions	Best
batch_size	32	256	64	-	64
learning_rate	5e-5	3e-2	0.5	-	3e-3
filter_size	3	7	2	-	3
num_filters	32	256	32	-	-
fc_per_layer	128	128	-	-	128
weight_init	-	-	-	glorot_uniform, glorot_normal	glorot_uniform
optimizer	-	-	-	tanh, relu	tanh
dropout	0.0	0.5	0.1	-	0.1 conv, 0.1 fc

Table 7: Hyper-parameter tuning ranges and best found parameters for sparse direct feedback alignment (SDFA).

Parameter	Range Min	Range Max	Increment	functions	Best
batch_size	32	256	32	-	32
learning_rate	5e-5	3e-2	0.5	-	4e-3
filter_size	3	7	2	-	3
num_filters	32	256	32	-	-
fc_per_layer	128	128	-	-	128
weight_init	-	-	-	glorot_uniform, glorot_normal	glorot_normal
optimizer	-	-	-	tanh, relu	relu
dropout	0.0	0.5	0.1	-	0.2 conv, 0.3 fc

Table 8: Hyper-parameter tuning ranges and best found parameters for random direct feedback alignment (RDFA).

## F Additional Results

We further present results on the fast gradient sign method (FGSM) and the Carnili and Wagner (C&W) attacks on the MNIST dataset. While we primarily focused on more natural image data in our tests in the main paper, we include MNIST results here in the Appendix for completeness. We also present additional images produced by FGSM and C&W for the Fashion MNIST dataset. Notably, as seen in Table 9, is consistently more robust to adversarial assault than backprop with respect to all four measured metrics.

Attack & Learning Mech.	Accuracy	Precision	Recall	F1 Score
FGSM BP	9.74	09.00	12.00	10.28
FGSM EKDAA	32.30	32.00	46.00	37.74
C&W BP	14.42	13.00	38.00	19.37
C&W EKDAA	85.30	85.00	85.00	85.00

Table 9: FGSM and C&W attack evaluation on backprop (BP) and EKDAA for the MNIST dataset. Accuracy, precision, recall, and F1-score are reported for the test images with the attacks applied.

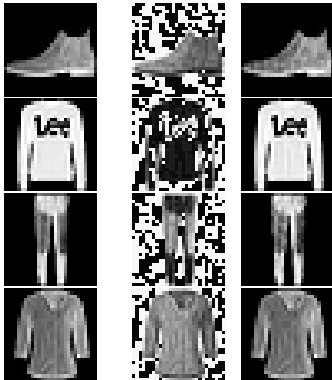


Figure 4: Adversarial image examples for the Fashion MNIST dataset. Original images (left) have the FGSM attack applied to them (middle) as well as the C&W attack (right).